



HAL
open science

High-temperature creep of single-crystal nickel-based superalloy: microstructural changes and effects of thermal cycling.

Bernard Viguiier, Fabienne Touratier, E. Andrieu

► **To cite this version:**

Bernard Viguiier, Fabienne Touratier, E. Andrieu. High-temperature creep of single-crystal nickel-based superalloy: microstructural changes and effects of thermal cycling.. Philosophical Magazine, 2011, pp.1. 10.1080/14786435.2011.609151 . hal-00743440

HAL Id: hal-00743440

<https://hal.science/hal-00743440>

Submitted on 19 Oct 2012

HAL is a multi-disciplinary open access archive for the deposit and dissemination of scientific research documents, whether they are published or not. The documents may come from teaching and research institutions in France or abroad, or from public or private research centers.

L'archive ouverte pluridisciplinaire **HAL**, est destinée au dépôt et à la diffusion de documents scientifiques de niveau recherche, publiés ou non, émanant des établissements d'enseignement et de recherche français ou étrangers, des laboratoires publics ou privés.



High-temperature creep of single-crystal nickel-based superalloy: microstructural changes and effects of thermal cycling.

Journal:	<i>Philosophical Magazine & Philosophical Magazine Letters</i>
Manuscript ID:	TPHM-11-Apr-0142.R1
Journal Selection:	Philosophical Magazine
Date Submitted by the Author:	20-Jul-2011
Complete List of Authors:	VIGUIER, Bernard; Université de Toulouse, CIRIMAT - INP/ENSIACET Touratier, Fabienne; Université de Toulouse, CIRIMAT - INP/ENSIACET Andrieu, E.; Université de Toulouse, CIRIMAT - INP/ENSIACET
Keywords:	Ni-based superalloys, dislocation mechanics, precipitation, microstructure change
Keywords (user supplied):	climb

SCHOLARONE™
Manuscripts

High-temperature creep of single-crystal nickel-based superalloy: microstructural changes and effects of thermal cycling.

Bernard Viguier, Fabienne Touratier and Eric Andrieu

Université de Toulouse, Institut Carnot CIRIMAT – INP/ENSIACET ; 4 allée Emile Monso, 31030 Toulouse Cedex 4, France.

Corresponding author: Bernard.Viguier@ensiacet.fr, tel (33) 5 34 32 34 31; fax: (33) 5 34 32 34 98.

Creep tests have been performed on MC2 single crystal superalloy at 950°C/200 MPa and 1150°C/80 MPa under isothermal and thermal cycling conditions with a tensile axis along the [001] direction. It is shown that the thermal cycles strongly affect the creep behaviour at 1150°C but not at 950°C. This was related to the repetitive precipitation and dissolution of γ' small rafts for the higher temperature, as revealed by quantitative characterisation of the γ/γ' microstructure. The dislocation microstructure exhibits similar trends in all the tested conditions, with a very high activity of a[100]-type dislocations climbing through the rafts. Such climbing dislocations constitute a recovery process for the deformation active system. It appeared that the density of a[100] dislocations, and not their climb velocity - or diffusion rate - is the key parameter for the control of creep rate. The thermal cycles which imply the creation and subsequent dissolution of rafts, provided new dislocations which explains the acceleration of creep observed under such conditions.

Keywords: anisothermal, creep, superalloy, MC2, climb, dislocations, rafting

1. Introduction

Single-crystal nickel-based superalloys are extensively used in the aeronautic industry, particularly in the hottest parts of turbo-reactors for aircraft and helicopters. The optimized microstructure consists of an array of γ' cubic precipitates aligned along the $\langle 100 \rangle$ cubic directions and coherently embedded in an austenitic matrix γ . Creep at high temperature leads to changes in this microstructure where cubes coarsen to form platelets in a direction perpendicular to the [001] tensile axis depending on the sign of the misfit: this is rafting [1]. The creep behavior of superalloys and the associated morphological changes have been extensively studied over the last 30 years but almost exclusively by means of isothermal creep tests [2-5]. Real service conditions in aircraft or helicopter engines, including certification tests, imply much

to be submitted to Phil Mag.

1
2
3 more severe thermo-mechanical loading of the superalloys, far from isothermal and
4 where temperatures can reach up to 1200°C during emergency regimes. Nevertheless,
5
6 very few studies have dealt with non isothermal creep [6-10]. Raffaitin et al. [6, 7]
7
8 studied the behavior of the superalloy MC2 with anisothermal creep at very high
9
10 temperatures. During thermal cycling creep tests under 1150°C and 80MPa, with
11
12 cycles composed of heating, high-temperature dwell and cooling steps, they reported
13
14 a creep behavior drastically different from that observed under isothermal loading,
15
16 reducing creep life 3- or 4-fold and increasing the secondary creep rate 10-fold.
17
18 Besides, a focus on the strain corresponding to each cycle underlines that it is not
19
20 linear but shows, at the beginning of the high-temperature dwell, a transient period
21
22 followed by a linear phase. This acceleration recalling a primary creep stage involves
23
24 the acceleration of the global creep rate; however, its origin has not yet been fully
25
26 elucidated.
27
28
29
30
31
32

33
34 Superalloy high-temperature isothermal creep is being increasingly studied
35
36 and results show the presence of $a\langle 010 \rangle$ prismatic edge dislocations aligned along
37
38 $\langle 110 \rangle$ directions and moving by climb within the rafts [11-20]. It has been observed
39
40 that the majority of these systems are $a[100]$ or $a[010]$ dislocations, so they
41
42 experience no force at all from the $[001]$ applied stress (their Schmid factor for glide
43
44 and climb is equal to 0). One way to explain climbing of such systems into the rafts
45
46 was proposed by Epishin et al. [16]. Their model consists in a vacancy exchange
47
48 between two different dislocation systems, moving by pure climb or by a combined
49
50 glide and climb process: the first is localized at the γ/γ' interface, takes part in the
51
52 interfacial network, and is composed of $a[001]$ dislocations activated by the applied
53
54 stress, while the second is composed of $a[100]$ and $a[010]$ dislocations, fed by the
55
56 vacancies from the first system. This mechanism was also investigated by Momprou
57
58
59
60

1
2
3 and Caillard to explain quasi-crystal deformation [21, 22]. The climbing of a[100]
4 type dislocations does not produce a creep strain along the load axis directly, but it is
5 an essential sequence of the global deformation mechanism occurring during the
6 secondary stage of nickel-based superalloy creep. Indeed when the superalloy
7 microstructure is fully rafted, the deformation can be limited to the γ corridors
8 otherwise dislocations would accumulate at the γ/γ' interface and strain would be
9 rapidly stopped. Steady-state deformation requires a recovery process for the
10 annihilation of the accumulated dislocations, which implies that the γ' rafts must be
11 crossed. The climb of [010] dislocations, even if it does not produce any deformation
12 along the [001] axis, can be considered as the limiting step of the global creep
13 mechanism.

14
15
16
17
18
19
20
21
22
23
24
25
26
27
28
29
30
31 The present study aims at improving our understanding of the fundamental
32 mechanisms occurring during high-temperature creep of single-crystal superalloys.
33 We focused our study on two scale levels. First the evolution of the γ/γ'
34 microstructure is studied during the creep tests with an emphasis on the changes
35 occurring during the imposed thermal cycle. Then the active dislocation systems are
36 characterized in order to elucidate the creep rate-controlling mechanism. Finally, the
37 high-temperature mechanisms will be discussed with regard to these results and the
38 consequences of thermal cycling conditions upon dislocation mechanism will be
39 examined.

40 41 42 43 44 45 46 47 48 49 50 51 52 53 54 55 **2. Experimental details**

56
57 The material for this study was the single crystal nickel-based superalloy MC2
58 (nominal composition in wt. % Ni-7.2Cr-8Co-2Mo-7W-5.5Al-1.3Ti-5.6Ta) provided
59
60

to be submitted to Phil Mag.

1
2
3
4 by Turbomeca in the form of a single crystal plate subjected to the standard
5
6 solutioning treatment: 3h at 1300°C. Flat thin-wall tensile creep specimens (3x20
7
8 mm² gage length, 1mm thick) were electro-discharge machined with the long axis of
9
10 the specimen along the [001] direction while the flat face was parallel to the (100)
11
12 plane. After cutting, the specimens were heat treated for 6h at 1080°C followed by air
13
14 cooling and 20h at 870°C then final air cooling. All the faces of the creep specimens
15
16 were ground with SiC paper, down to grade 4000 for the two large faces and grade
17
18 1000 for the edges, in order to remove the electro-discharge machine damaged zone.
19
20 It was checked that the initial microstructure consisted of cubic γ' precipitates (with a
21
22 440 nm mean edge length), well aligned along the $\langle 001 \rangle$ directions in the γ austenitic
23
24 matrix. Creep tests were performed at 950°C/200MPa and at 1150°C/80MPa along
25
26 the [001] direction under laboratory air on a creep frame loaded with a dead weight
27
28 (i.e. constant load conditions) equipped with a radiation furnace allowing fast
29
30 temperature changes. Isothermal and thermal cycling creep was studied, in both cases
31
32 the specimen was first heated to the high-temperature value (either 950 or 1150°C)
33
34 and then loaded by setting the required weight. The deformation was recorded using a
35
36 contact-less laser extensometer as described in detail in [23]. For thermal cycling
37
38 creep experiments, the temperature was monitored as shown in Figure 1: the cycle
39
40 duration was 60 minutes with a 5 minute heating stage up to 950 or 1150°C, a dwell
41
42 time of 30 minutes and a 25 minutes cooling stage (see below for the temperature
43
44 profile during the cooling step) down to about 45°C. The load was kept constant
45
46 during the thermal cycling.

47
48
49
50
51
52
53
54
55
56
57
58
59
60
Special care was taken in the way specimens were cooled for the interrupted tests. Indeed, this is of prime importance in order to get information on the evolution of the γ/γ' microstructure and specially the γ' dissolution phenomenon. First, we shall

to be submitted to Phil Mag.

1
2
3 consider the cooling rate that the sample experiences during the normal thermal cycle.
4
5 This is shown as the “slow” rate curve in Figure 2, it corresponds to a controlled
6
7 cooling rate of 3.75°C/s down to 600°C and then an even slower cooling rate due to
8
9 the furnace and load train thermal inertia. Some creep experiments were interrupted at
10
11 the end of such cooling steps for microstructure observations **which** are representative
12
13 of the low temperature state during the thermal cycle (point B in Figure1). Secondly,
14
15 some specimens were cooled as fast as possible, by suddenly switching off the
16
17 radiation furnace and opening the specimen chamber, so that the specimen is cooled
18
19 directly by laboratory air flow. This is illustrated by the “quench” curve in Figure 2,
20
21 and corresponds to a cooling rate of 33°C/s down to 800°C (the specimen cooled from
22
23 1150 to 850°C in 9 s). This cooling procedure was applied at the end and at the
24
25 beginning of the high-temperature dwell of the thermal cycles (points A and C
26
27 respectively in Figure 1). Finally some specimens were also cooled by switching off
28
29 the radiation furnace and letting the specimen cool down in the furnace, this gave an
30
31 intermediate cooling rate, labelled “fast” in Figure 2 and which was mainly used for
32
33 isothermal creep tests. After the creep tests, the specimens were mechanically ground,
34
35 first with SiC paper, then with diamond paste down to 1µm and finally etched with an
36
37 electrolytic solution (13% H₃PO₄, 45% H₂SO₄ and 42% HNO₃ under 3V) allowing γ
38
39 matrix dissolution. Scanning electron microscopy (SEM) was performed **with** a JEOL
40
41 JSM 6700 F equipped with a field emission gun operating at 15 kV using secondary
42
43 electron mode. The observations were made on the flat surface of the creep specimen.
44
45 In all SEM images reported the tensile axis [001] is vertical in the image plane – (100)
46
47 plane. Quantitative data on the γ' raft morphology were obtained using image analysis
48
49 of the SEM micrographs by Image J software [24]. The surface fraction of the rafts
50
51 was determined by manually redrawing the contour of rafts on seven images for each
52
53
54
55
56
57
58
59
60

to be submitted to Phil Mag.

1
2
3 experiment. Note that only rafts were considered, not the secondary precipitates
4
5 neither in spherical **nor in** cuboid shape. The thickness of the rafts and the periodicity
6
7 of the structure were measured along intercept lines drawn parallel to the [001]
8
9 direction, more details on such measurements are given in [25].
10
11

12
13 Thin foils for transmission electron microscopy (TEM) were sawn from thin
14
15 wall creep samples as squares 2.1 mm in length and 200 μm in thickness. These slices
16
17 were then mechanically polished down to about 50 μm while tilted in order to achieve
18
19 an orientation of the slice close to (211). The foils were then dimpled to about 20 μm
20
21 and ion milled using a Gatan PIPS $\text{\textcircled{R}}$ system. Dislocation observations for further
22
23 indexation were achieved in two-beam diffraction contrast on a Jeol 2010 operating at
24
25 200 kV at the TEMSCAN Service of University Paul Sabatier in Toulouse.
26
27
28
29
30

31 **3. Results**

32 **3.1 Mechanical behaviour**

33
34 The results of creep tests performed at 950°C/200 MPa and 1150°C/80 MPa are
35
36 shown in Figure 3 for isothermal and thermal cycling conditions. With thermal
37
38 cycling, the curves show only the deformation accumulated during the high-
39
40 temperature dwell, following the procedure described by Raffaitin et al. [6]. As
41
42 reported in Figure 3, the thermal cycling strongly affects the creep resistance at
43
44 1150°C, with a significant increase of the secondary creep rate and reduction of the
45
46 creep life duration. **The average secondary creep rate increases from $7.5 \cdot 10^{-8} \text{ s}^{-1}$ for**
47
48 **isothermal conditions to $4 \cdot 10^{-7} \text{ s}^{-1}$ in the present anisothermal creep conditions.** As
49
50 already noted [6] the strain produced during each high-temperature dwell is not a
51
52 linear function of the time but instead presents a slope change analogous to primary –
53
54 secondary creep stages as illustrated in **Figure 4.a**. The occurrence of this primary
55
56
57
58
59
60

1
2
3 stage for each cycle is believed to be responsible for the global creep acceleration.
4
5 Similar behaviour and the same occurrence of primary creep after a thermal change
6
7 was also reported by Cormier et al [9]. For comparison, isothermal and thermal
8
9 cycling creep experiments were conducted at 950°C, under 200 MPa. Due to the very
10
11 long creep life in those conditions the tests were not conducted to rupture but stopped
12
13 during the secondary stage. The curves shown in Figure 3 indicate that, for 950°C, the
14
15 thermal cycling did not affect the secondary creep rate. **Indeed the same average**
16
17 **secondary creep rate (10^{-8} s^{-1}) was measured for isothermal and anisothermal**
18
19 **conditions.** Furthermore close examination of the deformation curve of the thermal
20
21 cycling creep test shows that for each high-temperature dwell, the strain is a linear
22
23 function of time (constant creep rate), **see Figure 4.b,** unlike the primary and
24
25 secondary stages observed for thermal cycling creep at 1150°C. This observation
26
27 supports the link between the global creep acceleration due to thermal cycling at
28
29 1150°C and the occurrence of a primary creep stage for each dwell.
30
31
32
33
34
35
36

3.2 Microstructural characterisation

3.2.1 γ/γ' microstructure evolution

37
38
39
40
41 The microstructure of the crept specimens was investigated firstly at the γ/γ' scale
42
43 (SEM observations). Figure 5 shows the microstructure of specimens tested at 950°C
44
45 under isothermal and thermal cycling conditions, and interrupted after 117 and 147
46
47 hours respectively (time at high temperature). After creep interruption, the isothermal
48
49 sample was cooled using the “fast” procedure and the thermal cycling test was
50
51 interrupted at the low-temperature state of the cycle (corresponding to point B in
52
53 Figure 1). The microstructures showed a very clear rafted state as commonly observed
54
55 in the secondary creep stage [1]. Quantitative image analyses reveal a surface fraction
56
57 of the γ' phase of 75 and 73.5 % and raft thickness of 420 ± 20 and 405 ± 25 nm for
58
59
60

to be submitted to Phil Mag.

1
2
3 the isothermal and thermally cycled specimens respectively. Those values correspond
4
5 to a classical rafted structure in MC2 alloy under tensile creep at temperatures lower
6
7 than 1000°C. They indicate that γ' dissolution does not occur during exposure to
8
9 950°C whether in isothermal or cycling conditions.
10
11

12
13 In contrast, the microstructures observed on specimens crept at 1150°C under
14
15 isothermal figure 6(a) and thermal cycling tests figures 6(b to d) interrupted at
16
17 different points of the thermal cycle are quite different. The thermal cycling creep
18
19 tests were interrupted at the end of the 12th – beginning of 13th cycle, as schematised
20
21 in Figure 1. The first specimen, shown in Figure 6(b), corresponds to the interruption
22
23 of the test at the end of the 12th with a “quench” cooling; it is representative of point
24
25 A in Figure 1. The second specimen, Figure 6(c), also stopped at the end the 12th
26
27 cycle, was cooled with the “slow” procedure and thus represents low-temperature
28
29 point - B - of the thermal cycle. Finally the microstructure seen in Figure 6(d) is from
30
31 a sample that was “quenched” from the beginning of the 13th thermal cycle and
32
33 represents point C. These three specimens spent the same time (6 hours) at 1150°C
34
35 and experienced about 1% creep strain. For comparison the isothermal specimen,
36
37 shown in Figure 6(a), was also stopped after 1% creep strain, which in this case
38
39 corresponds to 14 hours spent at 1150°C. The general and common feature of the
40
41 microstructures observed in Figure 6 is the presence of large γ' precipitates – the rafts
42
43 – associated with smaller ones – secondary precipitates – within the γ corridors. It is
44
45 also apparently evident that the surface fraction of the rafts is much smaller than after
46
47 creep at 950°C. These observations indicate the role of γ' dissolution during creep at
48
49 1150°C, indeed for such temperatures the equilibrium volume fraction of γ' decreased
50
51 significantly [8]. A much more precise comparison of these microstructures was
52
53 obtained by quantitatively measuring the raft characteristics, in terms of raft surface
54
55
56
57
58
59
60

1
2
3 fraction (f_{sR}), raft thickness (t) and periodicity of the γ/γ' sequence (λ). The results of
4
5 these measurements, listed in Table 1, clearly reveal two main features: firstly a
6
7 difference between the isothermal and the anisothermal microstructures, and
8
9
10 secondly, an evolution of the microstructure during one thermal cycle. The most
11
12 important microstructural difference between isothermal and anisothermal creep
13
14 concerns the surface fraction of the rafts which was significantly lower for the
15
16 anisothermal creep ($f_{sR} = 40 - 47\%$) than for the isothermal ($f_{sR} = 56\%$), despite the
17
18 fact that anisothermal specimens spent less time at 1150°C than isothermal
19
20 specimens. The surface fraction of rafts also changed during one thermal cycle, since
21
22 it rose from about 40% for the high-temperature states (40% for point A and 42% for
23
24 C) to 47% for the low-temperature point B. This variation of raft surface fraction
25
26 already indicates that the thermal cycling enhanced the dissolution of γ' rafts, and that
27
28 during cycling, rafts continuously dissolved and reprecipitated. It also appears that the
29
30 raft thickness depends on the creep conditions. Indeed, after isothermal creep the
31
32 average thickness of the rafts was $t = 410$ nm, the same value was measured after
33
34 thermal cycling was interrupted at point C (beginning of the high-temperature dwell
35
36 during cycling creep) whereas the thickness was slightly lower for the low-
37
38 temperature point ($t = 400$ nm for point B) and significantly lower at the end of the
39
40 dwell ($t = 356$ nm for point A). The parameter λ also varied during the thermal cycle:
41
42 $\lambda = 908$ nm at the end of the dwell – point A – it dropped to 690 nm for the low-
43
44 temperature point –B – and increased back to 805 nm at the beginning of the
45
46 following dwell – point C. This parameter is correlated to the number of rafts present
47
48 in the microstructure, and its variations thus show that rafts are successively created
49
50 and dissolved during the thermal cycle.
51
52
53
54
55
56
57
58
59
60

to be submitted to Phil Mag.

1
2
3
4
5
6
7
8
9
10
11
12
13
14
15
16
17
18
19
20
21
22
23
24
25
26
27
28
29
30
31
32
33
34
35
36
37
38
39
40
41
42
43
44
45
46
47
48
49
50
51
52
53
54
55
56
57
58
59
60

Besides the variation of raft structure, secondary γ' precipitates are visible in the micrographs of Figure 6 in the γ matrix channels. These small precipitates are due to γ' phase dissolution during the high-temperature dwell and its re-precipitation during the cooling phase as is currently reported in the literature [26-28]. These secondary precipitates exhibit different morphologies and sizes, mainly depending on the cooling rate as shown in Figure 7. For rapid cooling, such as “quench” and “fast” procedures, the secondary precipitation consists in the homogeneous distribution of spherical precipitates with a diameter of around 30 nm, as exemplified in Figure 7(a). For the “slow” cooling rate, corresponding to point B in the thermal cycle, secondary precipitation forms cuboid precipitates with a mean edge length of 100 nm. Unlike the spheres, these cubes are not homogeneously distributed in the γ channels but are concentrated in the middle of the channel and surrounded by the γ phase containing fine spherical precipitates with 23 nm mean diameter Figure 7(b). Examination of the microstructure at a larger scale in the B state also reveals that some of the cuboid secondary precipitates coalesced to form new rafts, in agreement with the decrease of the period λ which was measured between states A and B.

If we now summarise the overall change of the γ' precipitates during a cycle of an anisothermal creep test at 1150°C, it can be noticed that during the cooling phase (A to B) the thickness of the rafts increased, the period of the structure decreased considerably and as a consequence, the surface fraction of the rafts increased. During the heating phase (B to C), the thickness of the rafts remained constant, the period of the structure increased but remained below the value of the state A and the surface fraction of the rafts decreased slightly. Finally, on the high-temperature dwell (C to A), the thickness of the rafts decreased, the period of the

to be submitted to Phil Mag.

1
2
3 structure increased and so, the surface fraction decreased. This will be discussed
4
5 below in terms of dissolution and reprecipitation of the γ' rafts and its consequences
6
7
8 on the creep behaviour during thermal cycling creep tests.
9

10 11 12 13 3.2.2 Dislocation microstructures 14

15
16 Dislocation microstructures were observed in the specimens crept in the different
17
18 conditions. Since we are working with rafted structures, recovery mechanisms of the γ
19
20 dislocations are required to allow macroscopic deformation of the superalloy. It has
21
22 been repeatedly proposed that such recovery may occur by dislocations crossing the γ'
23
24 rafts [29, 30]. Thus, we focus our study on the dislocation microstructure within the
25
26 rafts. A view of the dislocation landscape after creep under thermal cycling conditions
27
28 rafts. A view of the dislocation landscape after creep under thermal cycling conditions
29
30 at 950°C/200 MPa is shown in Figure 8. It is seen that γ channels contain only a few
31
32 dislocations (with a $\frac{1}{2}[110]$ type Burgers vector) related to interfacial dislocations. In
33
34 contrast, quite numerous, isolated dislocations can be seen in the γ' rafts. They either
35
36 go right across the rafts (dislocation 1 in Figure 8) or they form loops connected to
37
38 one side of the raft and which bow into the γ' raft (dislocation 2 in Figure 8). Similar
39
40 configurations were observed in specimens crept under isothermal conditions. A more
41
42 detailed analysis of different dislocation segments was performed on a specimen crept
43
44 under isothermal conditions at 1150°C/80 MPa. Figure 9 shows images of the same
45
46 area obtained with two different diffraction vectors. The whole analysis required the
47
48 use of up to seven different diffraction vectors; the direction of different dislocation
49
50 segments was determined using trace analysis on the foil stereographic projection.
51
52 Note that this analysis was made more complex by the fact that for dislocations with
53
54 Burgers vectors of the type $a[010]$ the $\mathbf{g}\cdot\mathbf{b} = 0$ criterion is not sufficient and quite a
55
56
57
58
59
60

to be submitted to Phil Mag.

1
2
3 strong residual contrast occurs when $\mathbf{g} \cdot \mathbf{b} \wedge \xi \neq 0$ as shown previously in the literature
4
5
6 [15, 31]. The results of such analysis are shown in Table 2, showing that the
7
8 dislocations present within the γ' raft have a[010] Burgers vector. Their line segment
9
10 is often parallel to $\langle 101 \rangle$ directions, so they are edge or 45° mixed dislocations.
11
12 Moreover, spatial configuration of dislocations, such as the segments labelled 4, 5 and
13
14 6 in Figure 9 show that they do not lie in their glide plane as showed in the scheme in
15
16 Figure 9.c. Such a spatial configuration could only be obtained by an intensive climb
17
18 process. A more general view of the dislocation landscape is shown in Figure 10, for a
19
20 specimen crept at $1150^\circ\text{C}/80\text{ MPa}$ under cycling conditions (the test was interrupted
21
22 after about 1% strain at point B – low temperature of the cycle). Results of similar
23
24 analysis performed on the different creep conditions show that, for all the creep
25
26 conditions that were studied (isothermal or anisothermal at 1150°C and 950°C), the
27
28 same type of dislocations was present within the rafts. They mainly consisted of
29
30 a[100] or a[010] edges or 45° dislocations aligned along the $\langle 101 \rangle$ directions and
31
32 sometimes some $a/2\langle 110 \rangle$ dislocations in the γ corridors, mainly at 950°C . For
33
34 $1150^\circ\text{C}/80\text{ MPa}$ conditions, the shape of these dislocations is prismatic with very
35
36 straight segments (Figures 9 and 10) whereas for $950^\circ\text{C}/200\text{ MPa}$, they are either
37
38 straight or rounded (Figure 8). Evidence of spatial configurations resulting from climb
39
40 was observed for all the conditions examined. We reported in Table the results of
41
42 rough estimate of the dislocation densities (based on the projected length of
43
44 dislocation lines in TEM micrograph without considering the projection correction
45
46 due to the different line orientations). It appears that a[010] type dislocations make up
47
48 not quite half of the total dislocations observed after creep at 950°C under cyclic
49
50 conditions whereas they were the more numerous after creep at 1150°C , especially for
51
52 creep under anisothermal conditions (this estimation does not take into account the
53
54
55
56
57
58
59
60

1
2
3 γ/γ' interfacial dislocations). Such measurements show the importance of climb of
4
5
6 a[010] dislocations during creep of the superalloy at such high temperatures.
7
8

9 **4. Discussion**

10 The creep behaviour of MC2 single crystal superalloy was studied at 950 and 1150°C
11
12 under isothermal and thermal cycling conditions. We showed that thermal cycling has
13
14 a tremendous effect on creep properties at 1150°C, with an acceleration of creep strain
15
16 and reduction of life-time, while the creep curves on each high-temperature dwell
17
18 exhibit a succession of primary and secondary creep stages. In contrast, the creep rate
19
20 does not seem to be affected by thermal cycling at 950°C and the individual creep
21
22 steps during high-temperature dwell show a monotonous increase of strain with time
23
24 (steady – state type creep). Two microstructural phenomena revealed in the present
25
26 study may play a significant role on creep behaviour at such high temperatures. These
27
28 are i) the evolution of γ' precipitates with dissolution-reprecipitation and ii) the climb
29
30 of $\mathbf{b} = a\langle 010 \rangle$ dislocations within the γ' rafts.
31
32
33
34
35
36
37
38
39

40 **4.1 Dissolution / reprecipitation of γ' phase**

41 The changes that occur in the γ/γ' microstructure during high-temperature
42
43 creep is of prime importance. The rafting phenomenon that transforms the initial
44
45 cuboid precipitate morphology into large plates has been studied for a many years [1,
46
47 3]. For moderate temperatures, as is the case in the present study for creep at 950°C,
48
49 this rafting occurs at constant γ' volume fraction as compared to the initial state. Only
50
51 very severe plastic deformation leads to destabilisation of the rafts during the tertiary
52
53 stage of the creep curve [32, 33]. However, for higher temperatures as is the case in
54
55 the present study of creep at 1150°C, dissolution of the γ' phase may occur [8, 34].
56
57
58
59
60

to be submitted to Phil Mag.

1
2
3
4 The first evidence of γ' dissolution is given by the values of the raft surface
5
6 fraction. Indeed in the initial microstructure, the surface fraction of γ' cuboids is about
7
8 70 %. This surface fraction does not change significantly after creep at 950°C either
9
10 under isothermal or cycling conditions. In contrast, creep at 1150°C involves a
11
12 decrease of the surface fraction down to 56 % for isothermal conditions and down to
13
14 about 40 % for thermal cycling creep. A direct consequence of γ' dissolution is to
15
16 create a supersaturated γ matrix that will lead to the formation of fine γ' secondary
17
18 precipitates upon cooling [35], such as those visible within the γ channels in the
19
20 micrographs in Figure 6. It is striking to observe the influence of the cooling rate on
21
22 secondary precipitate morphology as shown in Figure 7. Indeed the only difference
23
24 between samples A and B is the cooling rate: “quench” for A and “slow” for B,
25
26 according to the notation used in Figure 2. This precipitation has huge consequences
27
28 on the way the microstructure changes, since precipitation during the slow cooling
29
30 steps of the thermal cycles involves the creation of new small rafts as discussed
31
32 below.
33
34
35
36
37
38

39 From the microstructural study and the morphological data (Table 1) extracted from
40
41 interrupted thermal creep tests A, B and C at 1150°C/80MPa, we can propose the
42
43 following microstructural alterations during one thermal cycle. From A to B, this is
44
45 the slow rate cooling step, the period λ of the rafted structure significantly decreased
46
47 (from 910 to 690 nm) which means that new rafts appeared in the matrix corridors.
48
49 The new rafts were created during cooling by the coalescence of the cubic secondary
50
51 precipitates of the γ' phase, as observed in Figure 7(b). It is notable that the new rafts
52
53 are created very rapidly, since the time necessary to decrease the temperature from
54
55 1150 to 900°C is less than 90 s. From B to C, when the temperature was increased
56
57 from room temperature to 1150°C, the period of the structure increased (but λ is
58
59
60

to be submitted to Phil Mag.

1
2
3 lower at point C than it is at point A) which means that only one part of the rafts – the
4 smallest – formed during the cooling phase dissolved during reheating. This
5
6 dissolution of the smaller fresh rafts is supported by the complete dissolution of
7
8 cuboid secondary precipitates which is visible when comparing Figures 6(c) and 6(d).
9
10
11
12 This dissolution of the thinner rafts resulted in the cut off of the size distribution of
13
14 raft thickness for the smaller values which implied an increase of the mean value of
15
16 the distribution. Indeed during this heating step, the mean thickness of the rafts
17
18 increased slightly from 400 nm (point B at room temperature) to 410 nm (point C at
19
20 1150°C). It is even possible that during this step the thicker rafts were moderately
21
22 eroded but to a less extent than the small ones. This highlights the stability of the
23
24 larger rafts probably related to a very well established interfacial dislocation network.
25
26
27 Indeed the interfacial dislocation network does not appear to evolve along the thermal
28
29 cycle [36]. During the temperature dwell of the thermal cycle (from C to A), we can
30
31 note that the thickness of the rafts decreased and that the period of the structure
32
33 increased which means that the small rafts formed during the cooling step were totally
34
35 dissolved and that the larger ones began to dissolve slowly under the synergetic effect
36
37 of temperature and plastic strain.
38
39
40
41
42

43
44 During thermal cycling, not only very small spherical γ' precipitates, but also
45
46 cuboid ones and even small rafts are regularly created and dissolved. According to the
47
48 numbers given in Table 1, the precipitation kinetics were more rapid than the
49
50 dissolution kinetics, since the surface fraction (f_{sR}) and the number of rafts (through
51
52 the variation of λ) was higher at the point C than A. The low-temperature incursion
53
54 during creep creates new rafts, but on the other hand thermal cycling enhances global
55
56 γ' dissolution (overall raft surface fraction was always smaller in thermal cycling
57
58 conditions versus isothermal) and thus accelerates the creep damage [37]. This
59
60

to be submitted to Phil Mag.

1
2
3
4
5
6
7
8
9
10
11
12
13
14
15
16
17
18
19
20
21
22
23
24
25
26
27
28
29
30
31
32
33
34
35
36
37
38
39
40
41
42
43
44
45
46
47
48
49
50
51
52
53
54
55
56
57
58
59
60

apparent contradiction may be rationalised firstly by considering that imposing thermal cycling from the beginning of the creep hinders the stabilisation of numerous rafts and secondly by the synergetic effect between the microstructure evolution and creep strain. Indeed in superalloys the role of plastic strain, and the associated dislocation motion, on the transformation of the γ' microstructure has been repeatedly demonstrated either for formation of rafts [38] or for their destabilisation [32].

4.2 *Climb of $b = a\langle 010 \rangle$ dislocations*

We reported in section 3.2.2 the presence of numerous dislocations within γ' rafts with $a[010]$ Burgers vectors. This type of dislocation was the most frequent type observed after creep at the highest temperatures tested. Such $a[010]$ dislocation has been mentioned in earlier reports, in single-phase Ni_3Al compounds [39, 40] and in the γ' phase of the superalloy CMSX 2 [11, 12]. More recently they have been repeatedly observed to cut γ' rafts after high-temperature low-stress creep experiments in various superalloys: CMSX 6 [13], SRR 99 [14], CMSX 4 [29], CMSX 10 [16], TMS-138 [20]. In the last studies in which such dislocations were reported, in superalloys NASAIR-100 [19] and LEK94 [18], the authors recognised that this γ' cutting by climbing $a[100]$ dislocations is a generic recovery mechanism for high-temperature low-stress creep of superalloys. In line with these findings, we have shown that a similar mechanism also operates in MC2 superalloy, the activity of $a[010]$ dislocations being enhanced by the testing temperature as reported in Table 3. A common feature to most of these observations, from the literature and from the present study, is the fact that $a[010]$ dislocations move through a climb mechanism. It has been reported that the $a[100]$ dislocations may dissociate forming either

to be submitted to Phil Mag.

1
2
3 superpartial dislocations [29] or Shockley type partial dislocations involving stacking
4 faults [41] similarly to the configurations studied in other $L1_2$ compounds [42]. Such
5 dissociation seems to stabilize the line orientation along $\langle 101 \rangle$ directions, as
6 observed in the present study, but does not strongly impact the motion mode which is
7 still mainly climb. Even though to our knowledge, the sign of the climbing dislocation
8 has never been determined, it is postulated that $a[010]$ dislocations climb by
9 absorbing vacancies which results in shrinking the specimen (a climbing process
10 associated to the emission of vacancies would result in thickening the specimen in a
11 direction perpendicular to the applied tensile stress, which is not realistic).

12
13
14
15 The driving force for the activation of $a[010]$ dislocations has been questioned
16 in the literature. Indeed when creep load is imposed along the $[001]$ direction, the
17 $a[010]$ dislocations do not experience any resolved force (neither glide nor climb)
18 from the applied stress. It is thus believed that their activation is related to a kind of
19 secondary process that recovers the activation of a primary system which is actually
20 driven by the applied stress and provides creep strain along $[001]$. Such recovery
21 processes include i) the annihilation of γ/γ' interface dislocations when the $a[010]$
22 dislocations have crossed the raft [19] and ii) the absorption of vacancies emitted by
23 the climb of a primary system in the interface. Epishin and Link [16] were the first to
24 show that such a mechanism is involved in the high-temperature creep strain of
25 CMSX-4 and CMSX-10 superalloys. In their description, the creep strain along $[001]$
26 is due to the transverse glide-climb of $a/2\langle 011 \rangle$ dislocations, thus producing
27 vacancies. These excess vacancies can be absorbed by pores and by $a\langle 100 \rangle$
28 dislocations which implies their climb in γ' rafts. In turn, the crossing of rafts by
29 $a[100]$ dislocations annihilates interface dislocation, recovering the deformation
30 mechanism in the γ channels. Such a mechanism, involving two dislocation systems
31
32
33
34
35
36
37
38
39
40
41
42
43
44
45
46
47
48
49
50
51
52
53
54
55
56
57
58
59
60

to be submitted to Phil Mag.

1
2
3 and vacancy exchange has been demonstrated to operate during compression testing
4
5 of AlPdMn quasicrystals [21, 43]. The TEM observations reported here show that a
6
7 similar mechanism must operate in the MC2 superalloy single crystal during high-
8
9 temperature creep along the [001] axis.
10
11

12 This mechanism involves two dislocation systems: system 1 accounts for the
13
14 longitudinal strain along the load direction and creates vacancies, and system 2
15
16 absorbs vacancies and produces shrinkage of the specimen normal to the load axis.
17
18 Dislocation system 1 can ensure a steady-state macroscopic strain **only in the case**
19
20 **where the vacancies** it creates are eliminated in some way. If not, the osmotic force
21
22 due to the oversaturation of vacancies would block this deformation. The elimination
23
24 of vacancies requires two main points: i) the existence of sinks for the vacancies, and
25
26 ii) that the flux of vacancies to these sinks is fast enough compared to the strain rate.
27
28 These two points may be rate limiting and the creep rate of rafted single-crystal
29
30 superalloys could be controlled by the dislocations in γ' raft, either through their
31
32 limited climb velocity [29] or limited density [30]. We recently calculated [44] the
33
34 flux of vacancies generated by their diffusion between the γ/γ' interface (where an
35
36 oversaturation is due to the activity of system 1 dislocations) and the centre of γ' rafts
37
38 assumed to be at thermal equilibrium. The diffusion data show that for $T = 950^\circ\text{C}$ and
39
40 1150°C , this flux is more than large enough to ensure the transportation of vacancies
41
42 from system 1 to system 2 and thus can ensure condition ii) as stated above. The
43
44 thermal diffusion to pre-existing pores, which has been proposed as a alternative
45
46 vacancy sink [16], was shown to be much more difficult since the distance to be
47
48 travelled by the vacancies was in this case much larger than the raft thickness [44]. As
49
50 speculated in the literature [16, 30], we may assume that the density of sinks, that is
51
52 the density of system 2, climbing a[100] dislocations, may be the key point. This
53
54
55
56
57
58
59
60

1
2
3 hypothesis is supported by our thermal cycling results. Indeed, during the thermal
4
5 cycles the γ' phase repeatedly precipitates and dissolves. In particular, during the
6
7 cooling step we show that small rafts are formed, their rafted shape indicates that they
8
9 relaxed coherency stress, so they must be surrounded by a dislocation network for the
10
11 compensation of γ/γ' misfit. Such a coarsened secondary precipitate, formed during
12
13 anisothermal creep experiment – called micro-raft by the authors – has been indeed
14
15 observed to be surrounded by dislocations, see Figure 12 in [10]. Upon heating, these
16
17 rafts dissolve, we believe that the dislocations involved in the network are then
18
19 released and pushed apart by the applied stress (stress is maintained during the whole
20
21 cycle). By providing such fresh dislocations, the cooling step during thermal cycling
22
23 allows an acceleration of the creep strain at the beginning of the high temperature
24
25 dwell in the form of the primary stage, as observed in Figure 4 and in [6]. Once these
26
27 dislocations are exhausted, the creep rate is lowered, leading to the secondary stage in
28
29 the creep curve portion reported in Figure 4. Further support of the present conclusion
30
31 on the predominant role of dislocation density in the γ' raft to be used as vacancy
32
33 sinks is brought by the observation of samples crept at 950°C. In these conditions, the
34
35 γ' rafts are not dissolved, so no fresh dislocations are provided during creep, and a
36
37 close examination of the crept microstructure reveals the presence of numerous loops
38
39 inside the rafts, indicated by white arrows in Fig.11. The loops result from the
40
41 coalescence of oversaturated vacancies, that could not be eliminated by climbing
42
43 $a[100]$ dislocations.
44
45
46
47
48
49
50
51
52
53

54 Conclusions

55
56
57 The creep behaviour of the MC2 single-crystal superalloy was studied at very high
58
59 temperature, 950°/200 MPa and 1150°C/80 MPa under both isothermal and thermal
60

to be submitted to Phil Mag.

1
2
3 cycling conditions. It was shown that the thermal cycling strongly affects creep
4
5 behaviour at 1150°C while no effect was observed at 950°C, this was related to the
6
7 partial dissolution of the γ' phase for the highest temperatures. Indeed for 1150°C
8
9 testing, the thermal cycling during the creep test induces repeated precipitation and
10
11 dissolution of γ' particles, as secondary precipitates but also as small rafts. This
12
13 continuous modification of the precipitation microstructure during thermal cycles
14
15 alters the raft morphology by reducing the overall surface ratio of the rafts and
16
17 accelerating their degradation as compared to isothermal conditions.
18
19
20
21

22 The dislocation microstructures have been observed after interrupted
23
24 isothermal and thermal cycling creep tests. The role of a[100] dislocations crossing
25
26 the γ' rafts by a climbing process was revealed. This process acts as a recovery
27
28 mechanism **in regards to** the dislocations responsible for the strain along the loading
29
30 direction. This necessary recovery process could control the creep rate, however it
31
32 seems that diffusion rate or dislocation climb velocity is fast enough and may not be
33
34 rate limiting while the density of a[100] seems to be the crucial parameter. Thermal
35
36 cycling creep, through the dissolution of γ' rafts formed during the low temperature
37
38 incursion provides new dislocations which may explain the observed acceleration of
39
40 the creep rate.
41
42
43
44
45
46
47
48
49
50
51
52
53
54
55
56
57
58
59
60

Tables

Table 1: Quantitative characteristics of the rafted structure after creep at 1150°C/80 MPa in both isothermal and thermal cycling conditions. The surface fraction of the rafts (f_{sR}), their mean thickness (t) and the periodicity of the structure normal to the raft plane (λ) are given.

Table 2: Diffraction vectors – \mathbf{g} – and visibility of different dislocation segments shown in Figure 9, allowing their Burgers vector – \mathbf{b} - determination. For each segment the line direction – ξ – and the character – ϕ – were determined by stereographic analysis.

V: Visible, I: Invisible and RC: Residual Contrast.

Table 3 : Estimate of dislocation densities inside the γ' rafts separating dislocations with $\mathbf{b} = a[010]$ and other types of dislocations, depending on the creep conditions.

to be submitted to Phil Mag.

Figure Captions

Figure 1: Specimen temperature during thermal cycling creep experiments. Interrupted tests were stopped at three different points: i) at the end of the high-temperature dwell – point A; ii) at the low-temperature – point B; iii) at the beginning of the high temperature dwell – point C.

Figure 2: Specimen temperature showing the three different cooling rates (slow, fast and quench) used for interrupted tests.

Figure 3: Comparison of the creep curves obtained on isothermal and thermal cycling conditions for 950°C/200 MPa and 1150°C/80 MPa.

Figure 4: Details of the creep strain during one cycle (only the high-temperature dwell is shown) showing the primary–secondary stages for creep performed at 1150°C/80 MPa (a) and linear dependence of strain versus time for 950°C/200 MPa (b).

Figure 5: Microstructures after creep at 950°C/200MPa for isothermal (a) and thermal cycling (b) conditions.

Figure 6: Microstructures after creep at 1150°C/80 MPa for isothermal (a) and thermal cycling conditions. For the latter, tests were interrupted at different points of the thermal cycle, as indicated in Figure 1: point A, end of the 12th high temperature dwell (b); point B, low temperature point of the 12th cycle (c) and point C, beginning of the 13th high temperature dwell (d).

Figure 7: Details of the γ' secondary precipitation during creep at 1150°C the images correspond to cycling creep specimen interrupted at the end of the high-temperature dwell – point A – (a) and at the low temperature point – B- (b). Note that both samples only differ by the cooling rate from 1150°C to room temperature: “quench” for A and “slow” for B, as in the curves in Figure 2.

Figure 8: Dislocation microstructures in a specimen crept at 950°C / 200 MPa under thermal cycling conditions. Note dislocations (labelled 1 and 2) crossing or bowing into the γ' rafts and $a/2\langle 110 \rangle$ type dislocations in the γ corridors (labelled with X).

Figure 9: Example of diffraction contrast images used to identify the Burgers vector of the dislocations observed in the γ' rafts. The corresponding specimen was crept at 1150°C/80 MPa under isothermal conditions to rupture. The dislocations are imaged in BF two beam conditions with different diffraction vectors in (a) and (b). The

to be submitted to Phil Mag.

1
2
3
4
5
6
7
8
9
10
11
12
13
14
15
16
17
18
19
20
21
22
23
24
25
26
27
28
29
30
31
32
33
34
35
36
37
38
39
40
41
42
43
44
45
46
47
48
49
50
51
52
53
54
55
56
57
58
59
60

scheme in (c) illustrates the geometrical configuration of the dislocation segments 5,4,6 (thick black line) together with the cubic unit directions $\langle 100 \rangle$ (thin grey lines and cubes). The Burgers vector $b = a[010]$ of the dislocation is also indicated.

Figure 10: Overview of the dislocation microstructures in a specimen crept at 1150°C/80 MPa under thermal cycling conditions. The creep test was stopped at the low-temperature step of the thermal cycle (point B in Figure 2).

Figure 11: Detail of the dislocation microstructure in a specimen crept at 950°C/200 MPa under thermal cycling conditions – interrupted at low-temperature point of the thermal cycle - showing the presence of dislocation loops within the γ' rafts.

to be submitted to Phil Mag.

Acknowledgments

The authors would like to thank the company Safran-Turbomeca for providing the materials studied and for financial support.

References

- [1] F.R.N. Nabarro and H.L. De Villiers, *The physics of creep*. Taylor & Francis, London, 1995.
- [2] M. Feller-Kniepmeier and T. Link, *Metallurgical Transactions*, **20A** (1989) p. 1233.
- [3] T.M. Pollock and A.S. Argon, *Acta Metallurgica and Materialia*, **42** (1994) p. 1859.
- [4] V. Sass and M. Feller-Kniepmeier, *Materials Science and Engineering A*, **245** (1998) p. 19.
- [5] M. Kolbe, A. Dlouhy, and G. Eggeler, *Materials Science and Engineering A*, **246** (1998) p. 133.
- [6] A. Raffaitin, D. Monceau, F. Crabos, and E. Andrieu, *Scripta Materialia*, **56** (2007) p. 277.
- [7] A. Raffaitin, *Influence du cyclage thermique sur les comportements en oxydation/corrosion et en fluage de systèmes MCrAlY/superalliage à base de nickel*. PhD Thesis. Institut National Polytechnique de Toulouse. Toulouse: 2007.
- [8] J. Cormier, X. Milhet, and J. Mendez, *Journal of Materials Science*, **42** (2007) p. 7780.
- [9] J. Cormier, X. Milhet, J.L. Champion, and J. Mendez, *Advanced Engineering Materials*, **10** (2008) p. 56.
- [10] J.B. le Graverend, J. Cormier, M. Jouiad, F. Gallerneau, P. Paulmier, and F. Hamon, *Materials Science and Engineering: A*, **527** (2010) p. 5295.
- [11] F. Louchet and M. Ignat, *Acta Metallurgica*, **34** (1986) p. 1681.
- [12] R. Bonnet and A. Ati, *Acta Metallurgica*, **37** (1989) p. 2153.
- [13] G. Eggeler and A. Dlouhy, *Acta Materialia*, **45** (1997) p. 4251.
- [14] T. Link, A. Epishin, and U. Bruckner, *Scripta Materialia*, **39** (1998) p. 1463.
- [15] T. Link, A. Epishin, M. Klaus, U. Bruckner, and A. Reznicek, *Materials Science and Engineering A*, **405** (2005) p. 254.
- [16] A. Epishin and T. Link, *Philosophical Magazine*, **84** (2004) p. 1979.
- [17] A. Kostka, G. Malzer, and G. Eggeler, *Journal of Microscopy*, **223** (2006) p. 295.
- [18] A. Kostka, G. Malzer, G. Eggeler, A. Dlouhy, S. Reese, and T. Mack, *Journal of Materials Science* **42** (2007) p. 3951.

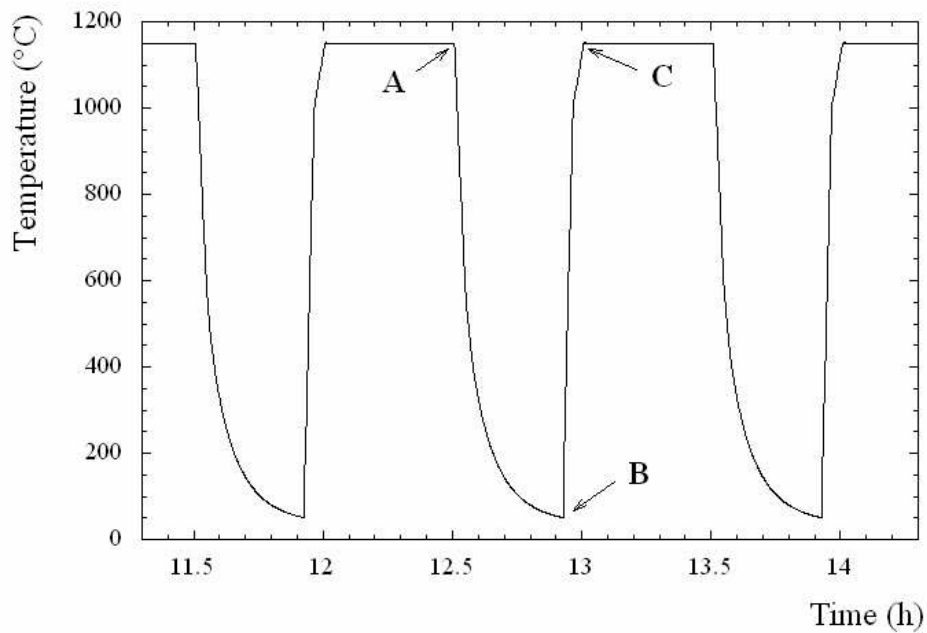
- 1
2
3
4 [19] P.M. Sarosi, R. Srinivasan, G.F. Eggeler, M.V. Nathal, and M.J. Mills, *Acta Materialia*, **55** (2007) p. 2509.
5
6 [20] J.X. Zhang, H. Harada, and Y. Koizumi, *Journal of Materials Research*, **21**
7 (2006) p. 647.
8 [21] F. Mompiau and D. Caillard, *Acta Materialia*, **56** (2008) p. 2262.
9 [22] F. Mompiau and D. Caillard, *Materials Science and Engineering A*, **483 - 484**
10 (2008) p. 143.
11 [23] S. Dryepontd, D. Monceau, F. Crabos, and E. Andrieu, *Acta Materialia*, **53**
12 (2005) p. 4199.
13 [24] ImageJ. *software available at* <http://rsbweb.nih.gov/ij/>
14 [25] F. Touratier, *Etude des mécanismes de déformation et d'endommagement du*
15 *superalliage base nickel MC2 en fluage aux très hautes températures*. PhD
16 Thesis, Institut National Polytechnique. Université de Toulouse.Toulouse:
17 2008.
18 [26] T. Grosdidier, A. Hazotte, and A. Simon, *Materials Science and Engineering*
19 *A*, **256** (1998) p. 183.
20 [27] A.M. Brass, D. Roux, and J. Chêne, *Materials Science and Engineering A*, **323**
21 (2002) p. 97.
22 [28] J. Cormier, X. Milhet, and J. Mendez, *Acta Materialia*, **55** (2007) p. 6250.
23 [29] R. Srinivasan, G.F. Eggeler, and M.J. Mills, *Acta Materialia*, **48** (2000) p.
24 4867.
25 [30] L.J. Carroll, Q. Feng, and T.M. Pollock, *Metallurgical and Materials*
26 *Transactions A*, **39** (2008) p. 1290.
27 [31] A. Dlouhy, R. Schaublin, and G. Eggeler, *Scripta Materialia*, **39** (1998) p.
28 1325.
29 [32] F. Touratier, E. Andrieu, D. Poquillon, and B. Viguier, *Mater. Sci. Eng. A-*
30 *Struct. Mater. Prop. Microstruct. Process.*, **510-11** (2009) p. 244.
31 [33] R.C. Reed, D.C. Cox, and C.M.F. Rae, *Materials Science and Engineering: A*,
32 **448** (2007) p. 88.
33 [34] K. Serin, G. Gobekli, and G. Eggeler, *Materials Science and Engineering A*,
34 **387-389** (2004) p. 133.
35 [35] T. Grosdidier, A. Hazotte, and A. Simon, *Scripta Metallurgica et Materialia*,
36 **30** (1994) p. 1257.
37 [36] M. Hantcherli, B. Viguier, F. Pettinari- Sturmel, J. Douin, and A. Coujou, to
38 be published, (2011).
39 [37] R. Goti, B. Viguier, and F. Crabos, to be published (2011).
40 [38] M. Veron, Y. Brechet, and F. Louchet, *Scripta Materialia*, **34** (1996) p. 1883.
41 [39] P. Veyssiere and J. Douin, *Philosophical Magazine*, **51** (1985) p. L1.
42 [40] N.L. Baluc, *Contribution à l'étude des défauts et de la plasticité d'un composé*
43 *intermetallique ordonné : Ni₃Al*. PhD Thesis, Ecole Polytechnique
44 Fédérale.Lausanne: 1990.
45 [41] C. Kohler, T. Link, and A. Epishin, *Philosophical Magazine*, **86** (2006) p.
46 5103.
47 [42] J. Bonneville and G. Vanderschaeve, *Philos. Mag. Lett.*, **78** (1998) p. 87.
48 [43] F. Monpiou, L. Bresson, P. Cordier, and D. Caillard, *Philosophical Magazine*,
49 **83** (2003) p. 3133.
50 [44] F. Touratier, B. Viguier, C. Siret, S. Lesterlin, and E. Andrieu, *Advanced*
51 *Materials Research* **278** (2011) p 7.
52
53
54
55
56
57
58
59
60

Creep condition and interruption point		f_{sR} (%)	t (nm)	λ (nm)
Isothermal		56±3	410±35	560±20
Thermal cycling	End of dwell (A)	40±4	356±35	908±30
	Low temperature state (B)	47±1	400±20	690±15
	Beginning of dwell (C)	42±5	410±25	805±20

		diffraction vector						b	ξ	φ	
		111	$11\bar{1}$	220	202	$20\bar{2}$	$00\bar{2}$				$\bar{2}00$
dislocation segment	1	V	V	V	RC	I	RC	RC	a[010]	$[10\bar{1}]$	90°
	2	V	V	V	RC	I	RC	RC	a[010]	$[10\bar{1}]$	90°
	3	V	V	V	RC	RC	RC	I	a[010]	[110]	45°
	4	V	V	V	RC	RC	RC	I	a[010]	[110]	45°
	5	V	V	V	I	RC	RC	RC	a[010]	[101]	90°
	6	V	V	V	RC	I	RC	RC	a[010]	$[10\bar{1}]$	90°
	7	V	I	V	V	I	V	V	a/2[101]	[101]	0°

Creep conditions	$b = a[010]$ density (m^{-2})	Other dislocations density (m^{-2})	Ratio of dislocation density
950°C/200MPa Isothermal	$0.66 \cdot 10^{12}$	$0.42 \cdot 10^{12}$	1.6
950°C/200 MPa Thermal cycling, point B	$1.64 \cdot 10^{12}$	$2.05 \cdot 10^{12}$	0.8
1150°C/80 MPa Isothermal	$1.45 \cdot 10^{12}$	$0.66 \cdot 10^{12}$	2.2
1150°C/80 MPa Thermal cycling, point B	$1.59 \cdot 10^{12}$	$0.22 \cdot 10^{12}$	7.2

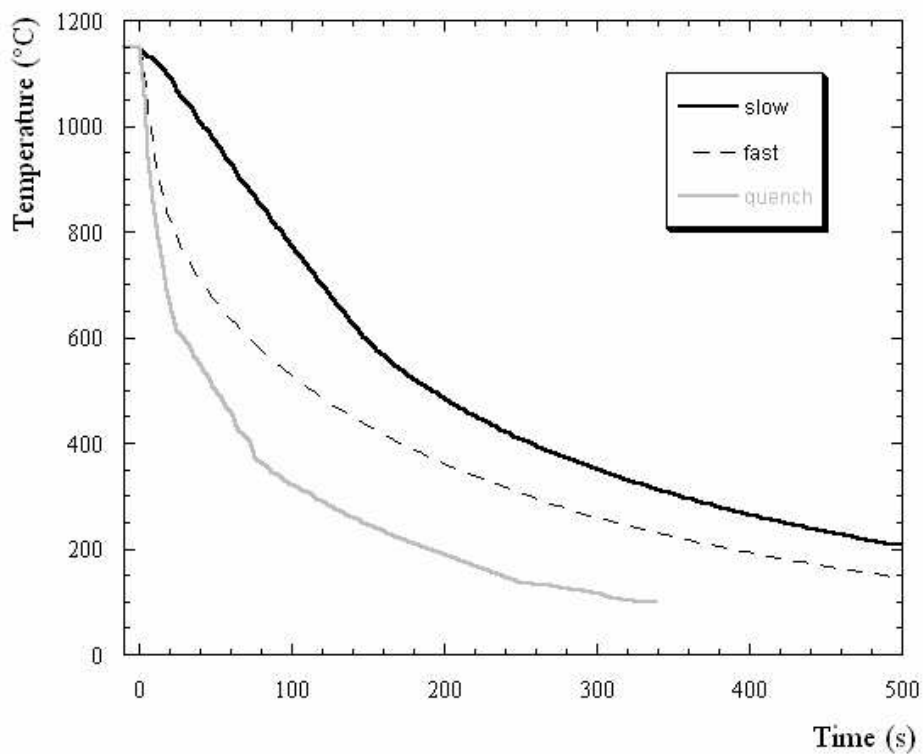
1
2
3
4
5
6
7
8
9
10
11
12
13
14
15
16
17
18
19
20
21
22
23
24
25
26
27
28
29
30
31
32
33
34
35
36
37
38
39
40
41
42
43
44
45
46
47
48
49
50
51
52
53
54
55
56
57
58
59
60



256x174mm (72 x 72 DPI)

Review Only

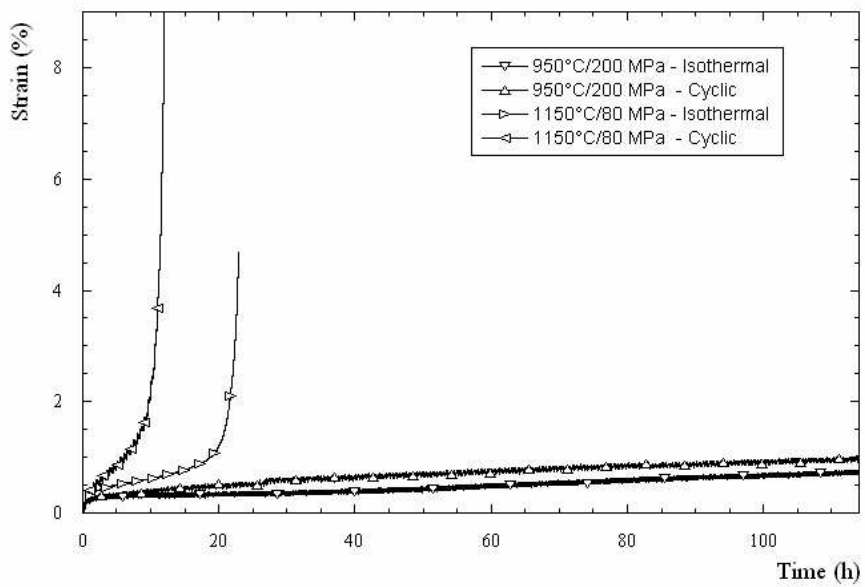
1
2
3
4
5
6
7
8
9
10
11
12
13
14
15
16
17
18
19
20
21
22
23
24
25
26
27
28
29
30
31
32
33
34
35
36
37
38
39
40
41
42
43
44
45
46
47
48
49
50
51
52
53
54
55
56
57
58
59
60



208x173mm (72 x 72 DPI)

Preview Only

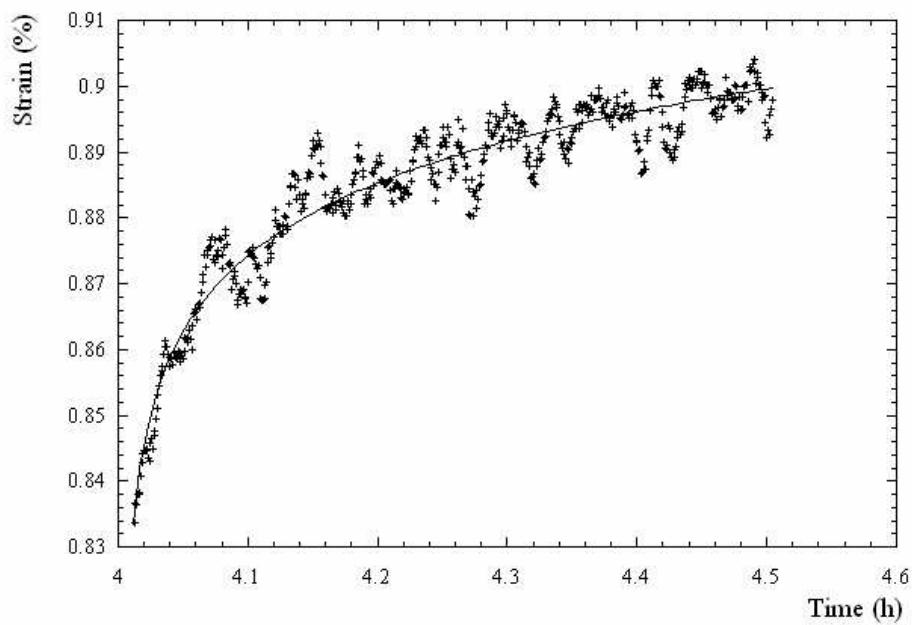
1
2
3
4
5
6
7
8
9
10
11
12
13
14
15
16
17
18
19
20
21
22
23
24
25
26
27
28
29
30
31
32
33
34
35
36
37
38
39
40
41
42
43
44
45
46
47
48
49
50
51
52
53
54
55
56
57
58
59
60



264x174mm (72 x 72 DPI)

Review Only

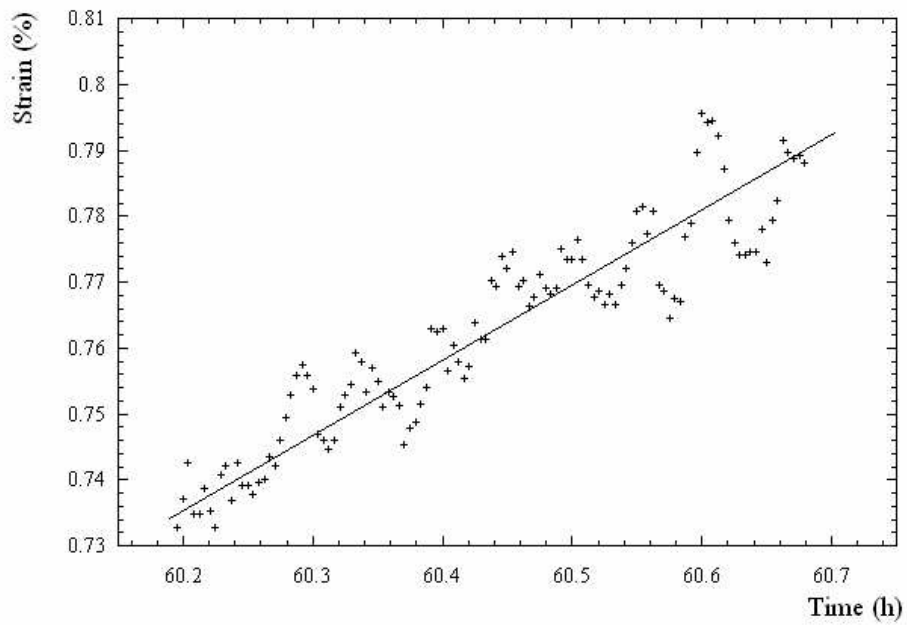
1
2
3
4
5
6
7
8
9
10
11
12
13
14
15
16
17
18
19
20
21
22
23
24
25
26
27
28
29
30
31
32
33
34
35
36
37
38
39
40
41
42
43
44
45
46
47
48
49
50
51
52
53
54
55
56
57
58
59
60



233x162mm (72 x 72 DPI)

Review Only

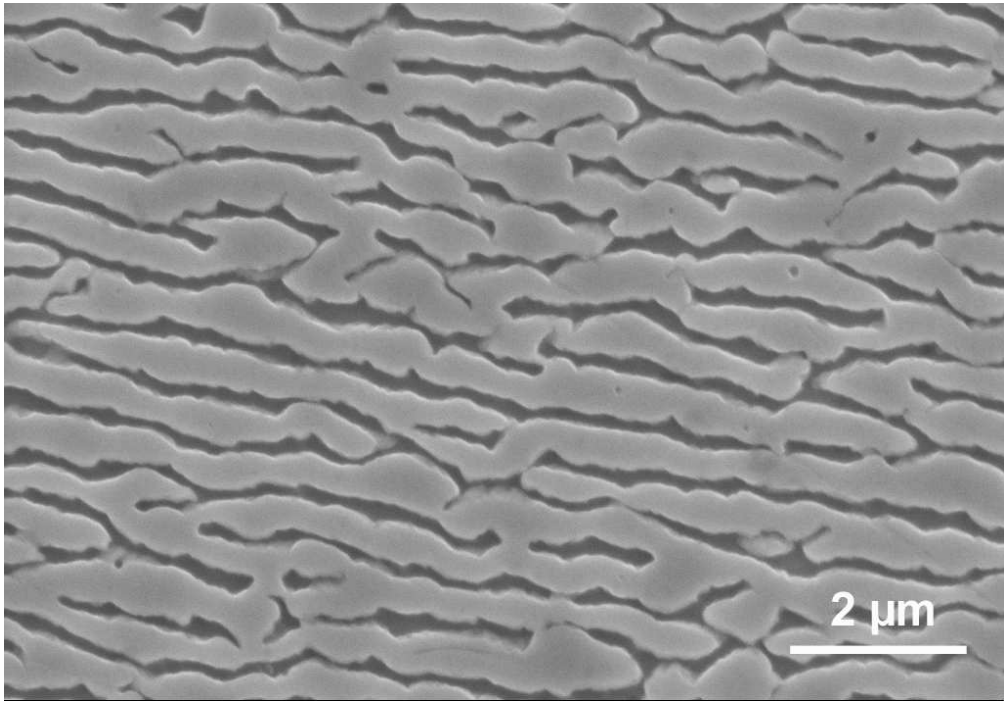
1
2
3
4
5
6
7
8
9
10
11
12
13
14
15
16
17
18
19
20
21
22
23
24
25
26
27
28
29
30
31
32
33
34
35
36
37
38
39
40
41
42
43
44
45
46
47
48
49
50
51
52
53
54
55
56
57
58
59
60



233x162mm (72 x 72 DPI)

Review Only

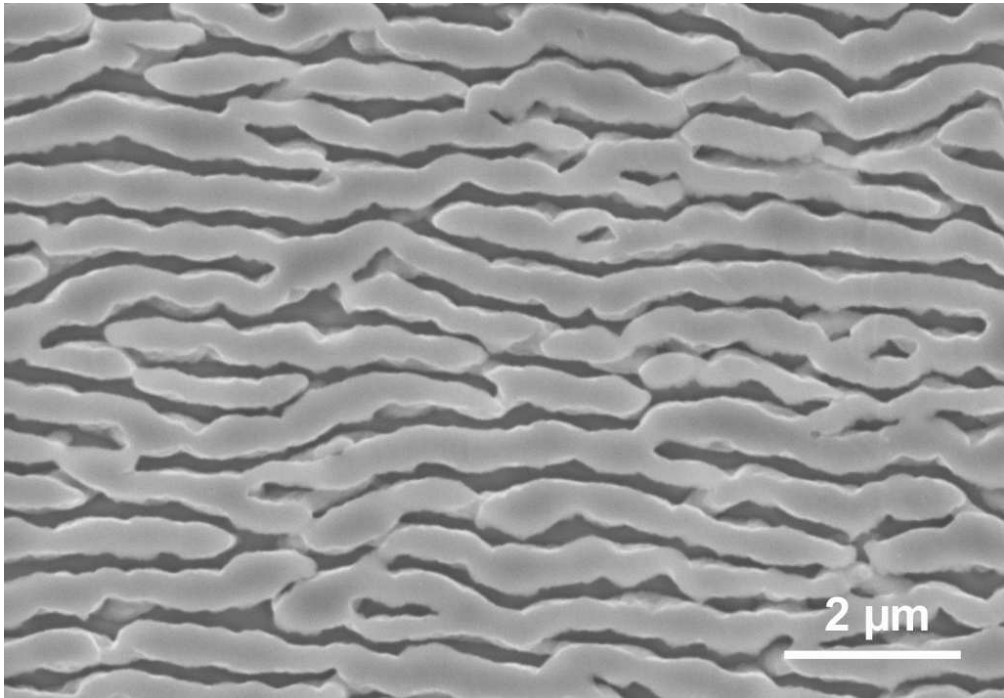
1
2
3
4
5
6
7
8
9
10
11
12
13
14
15
16
17
18
19
20
21
22
23
24
25
26
27
28
29
30
31
32
33
34
35
36
37
38
39
40
41
42
43
44
45
46
47
48
49
50
51
52
53
54
55
56
57
58
59
60



173x120mm (150 x 150 DPI)

view Only

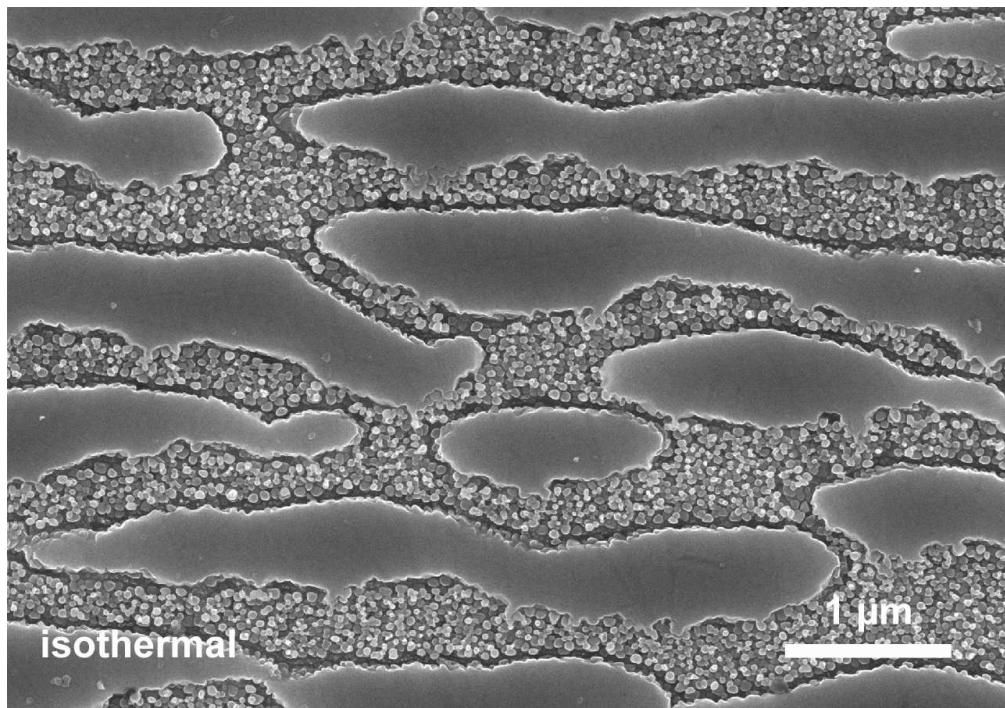
1
2
3
4
5
6
7
8
9
10
11
12
13
14
15
16
17
18
19
20
21
22
23
24
25
26
27
28
29
30
31
32
33
34
35
36
37
38
39
40
41
42
43
44
45
46
47
48
49
50
51
52
53
54
55
56
57
58
59
60



173x120mm (150 x 150 DPI)

Review Only

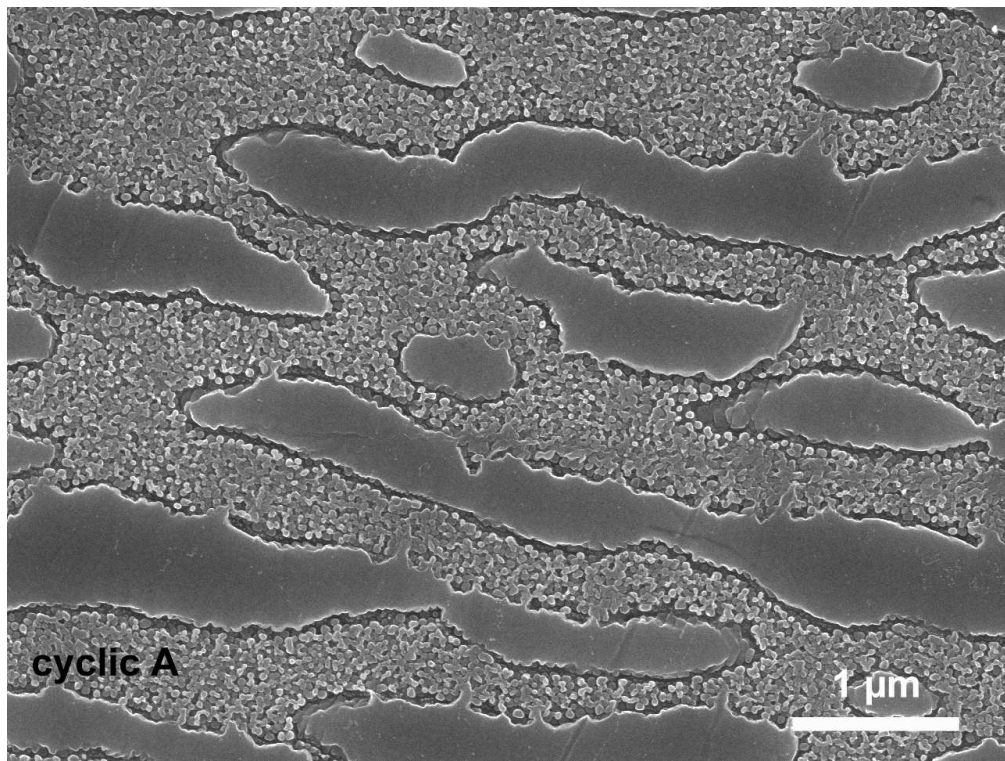
1
2
3
4
5
6
7
8
9
10
11
12
13
14
15
16
17
18
19
20
21
22
23
24
25
26
27
28
29
30
31
32
33
34
35
36
37
38
39
40
41
42
43
44
45
46
47
48
49
50
51
52
53
54
55
56
57
58
59
60



216x152mm (150 x 150 DPI)

view Only

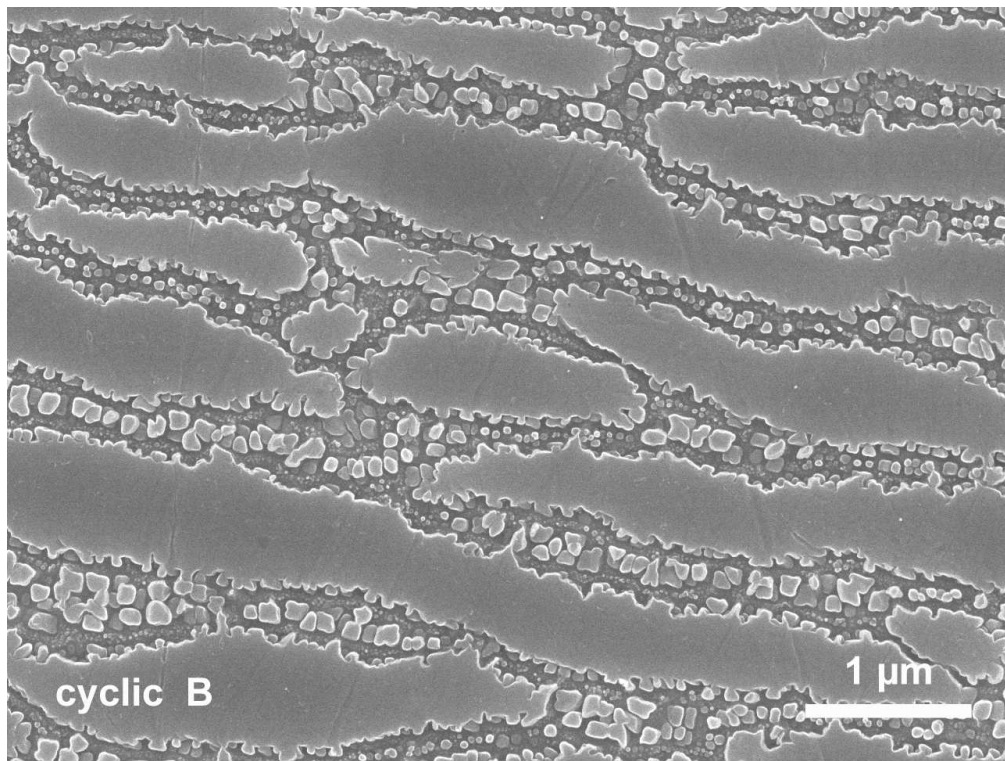
1
2
3
4
5
6
7
8
9
10
11
12
13
14
15
16
17
18
19
20
21
22
23
24
25
26
27
28
29
30
31
32
33
34
35
36
37
38
39
40
41
42
43
44
45
46
47
48
49
50
51
52
53
54
55
56
57
58
59
60



216x163mm (150 x 150 DPI)

View Only

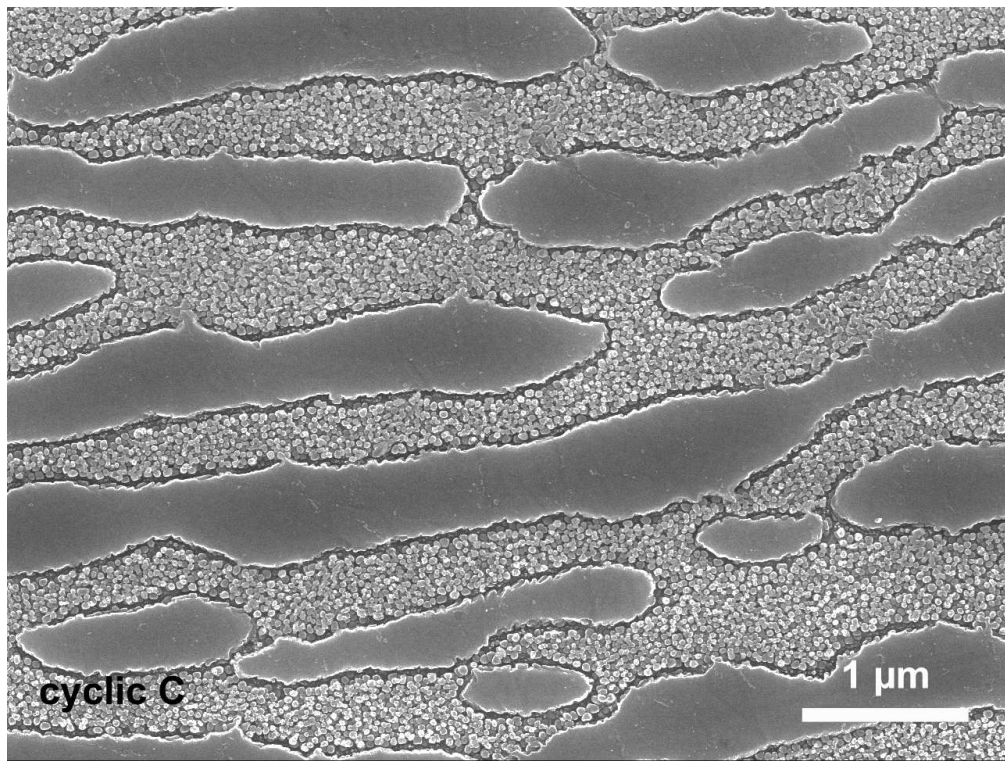
1
2
3
4
5
6
7
8
9
10
11
12
13
14
15
16
17
18
19
20
21
22
23
24
25
26
27
28
29
30
31
32
33
34
35
36
37
38
39
40
41
42
43
44
45
46
47
48
49
50
51
52
53
54
55
56
57
58
59
60



216x163mm (150 x 150 DPI)

View Only

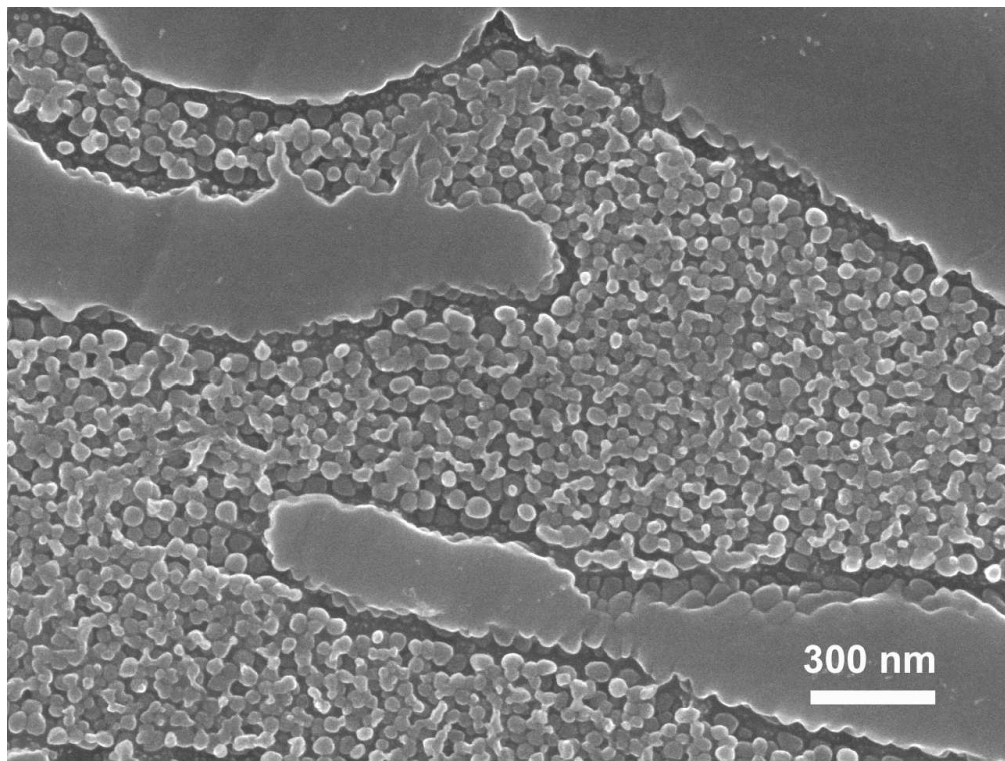
1
2
3
4
5
6
7
8
9
10
11
12
13
14
15
16
17
18
19
20
21
22
23
24
25
26
27
28
29
30
31
32
33
34
35
36
37
38
39
40
41
42
43
44
45
46
47
48
49
50
51
52
53
54
55
56
57
58
59
60



216x163mm (150 x 150 DPI)

View Only

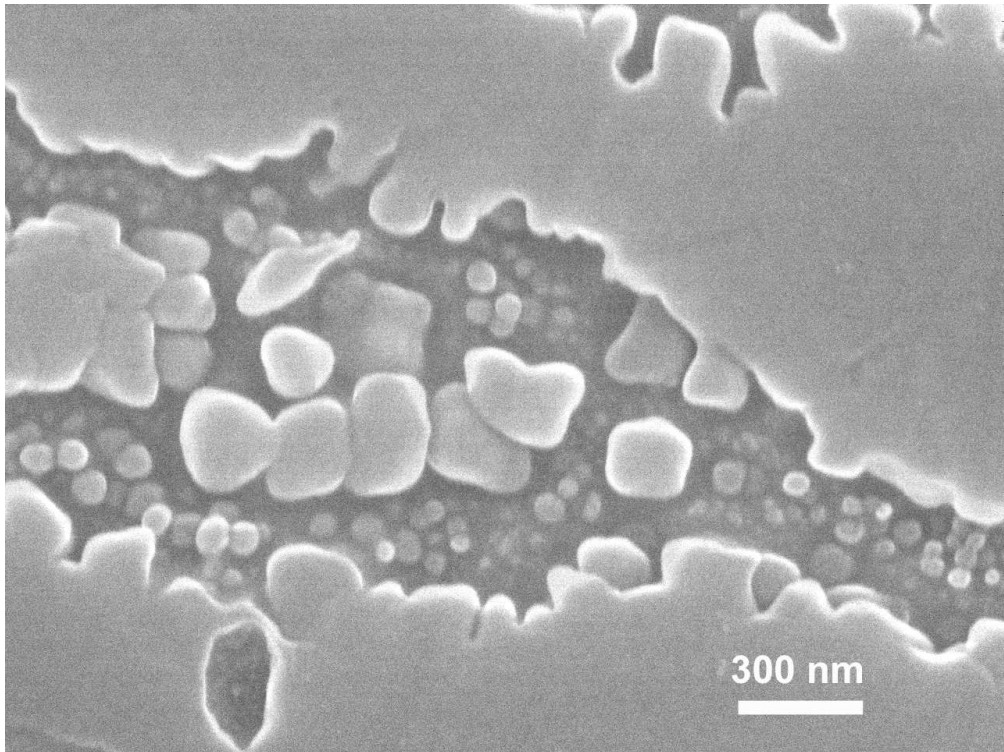
1
2
3
4
5
6
7
8
9
10
11
12
13
14
15
16
17
18
19
20
21
22
23
24
25
26
27
28
29
30
31
32
33
34
35
36
37
38
39
40
41
42
43
44
45
46
47
48
49
50
51
52
53
54
55
56
57
58
59
60



216x163mm (150 x 150 DPI)

View Only

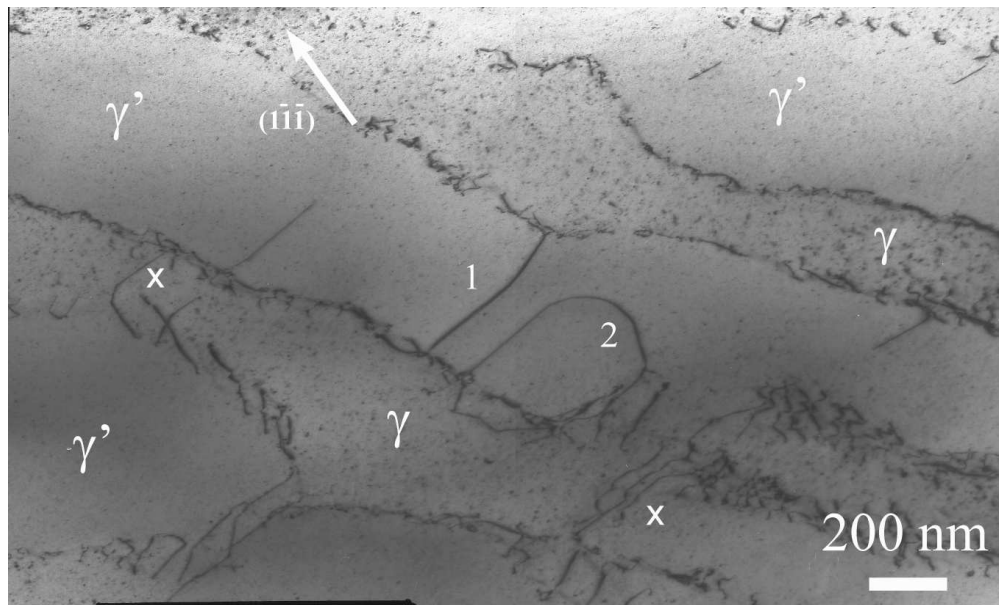
1
2
3
4
5
6
7
8
9
10
11
12
13
14
15
16
17
18
19
20
21
22
23
24
25
26
27
28
29
30
31
32
33
34
35
36
37
38
39
40
41
42
43
44
45
46
47
48
49
50
51
52
53
54
55
56
57
58
59
60



216x162mm (150 x 150 DPI)

View Only

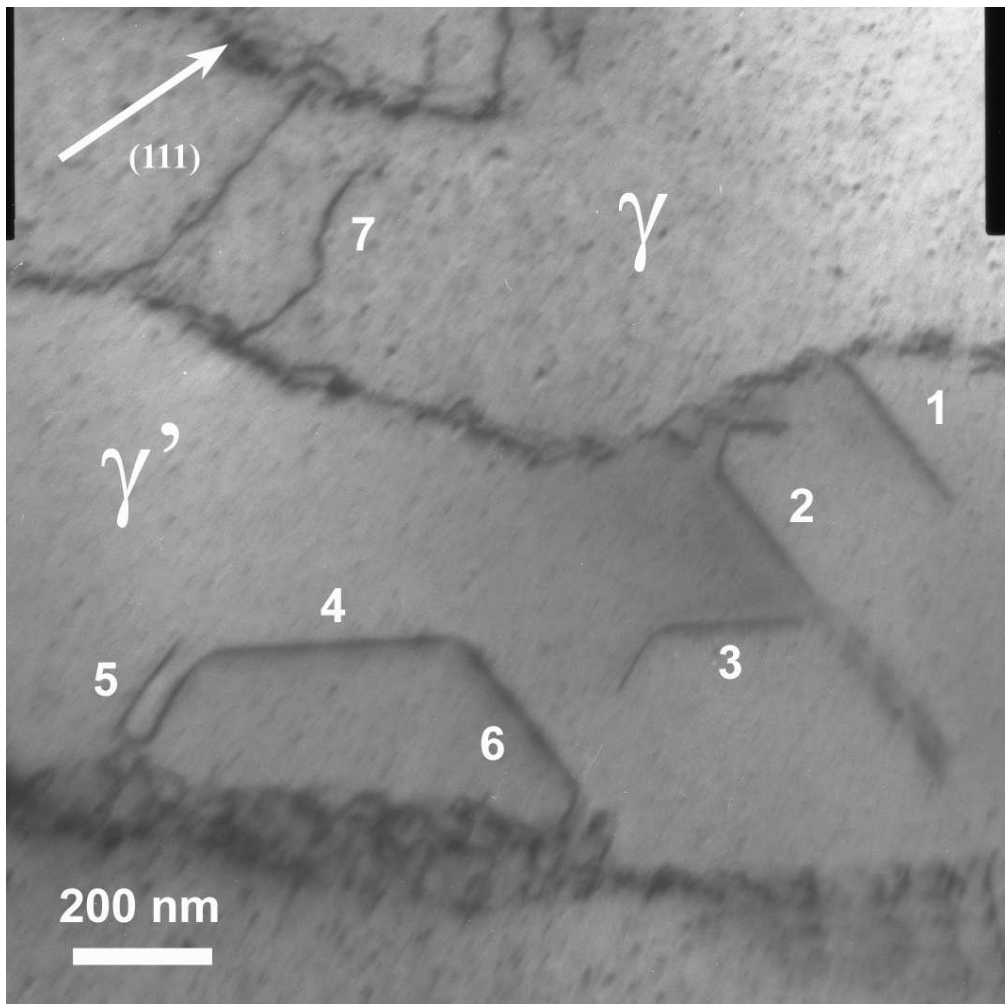
1
2
3
4
5
6
7
8
9
10
11
12
13
14
15
16
17
18
19
20
21
22
23
24
25
26
27
28
29
30
31
32
33
34
35
36
37
38
39
40
41
42
43
44
45
46
47
48
49
50
51
52
53
54
55
56
57
58
59
60



230x139mm (150 x 150 DPI)

Review Only

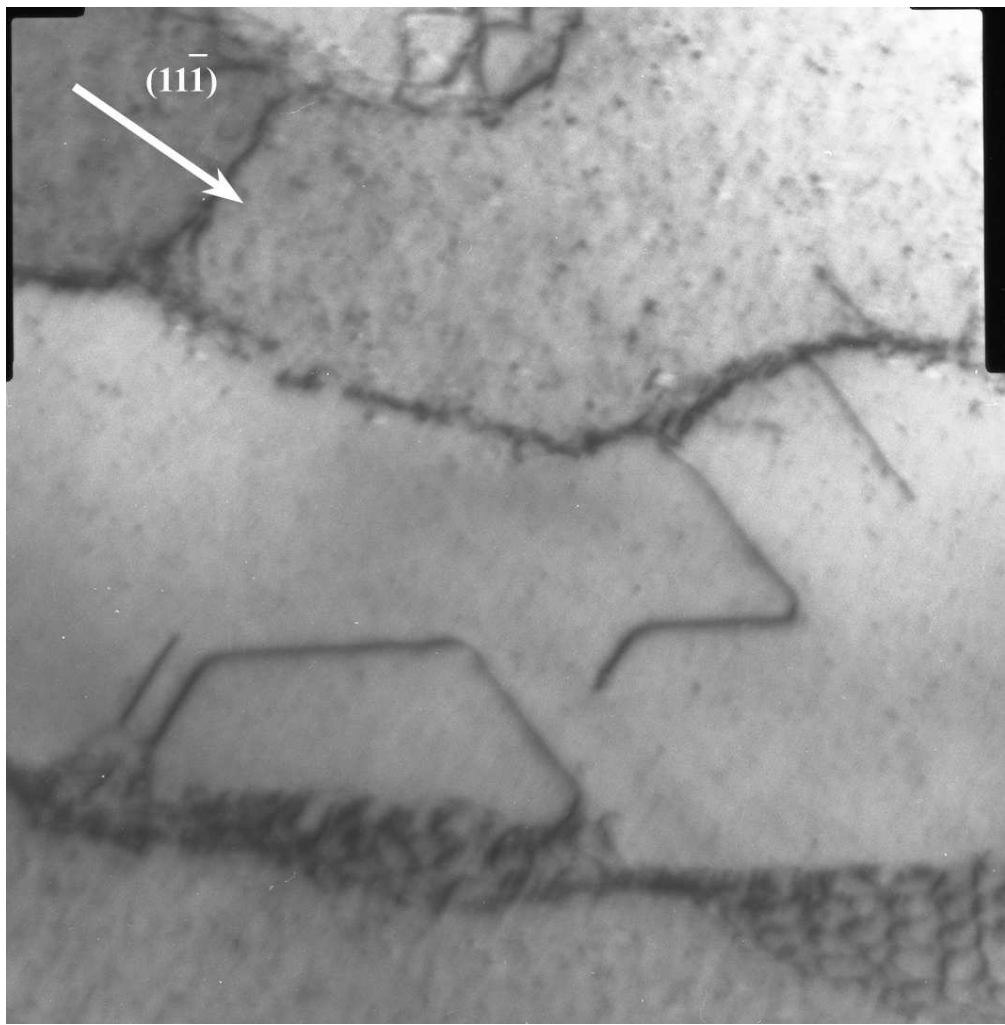
1
2
3
4
5
6
7
8
9
10
11
12
13
14
15
16
17
18
19
20
21
22
23
24
25
26
27
28
29
30
31
32
33
34
35
36
37
38
39
40
41
42
43
44
45
46
47
48
49
50
51
52
53
54
55
56
57
58
59
60



180x179mm (150 x 150 DPI)

only

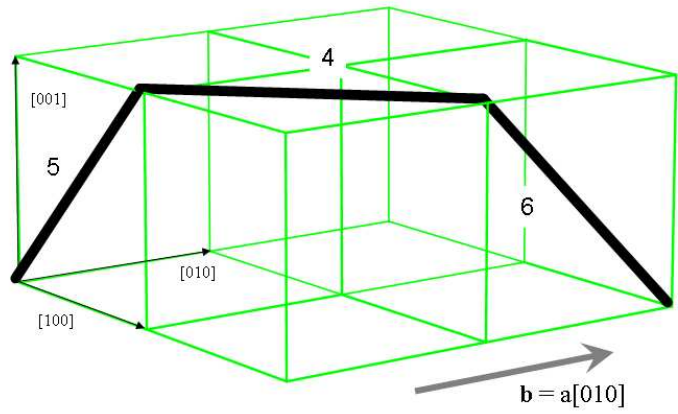
1
2
3
4
5
6
7
8
9
10
11
12
13
14
15
16
17
18
19
20
21
22
23
24
25
26
27
28
29
30
31
32
33
34
35
36
37
38
39
40
41
42
43
44
45
46
47
48
49
50
51
52
53
54
55
56
57
58
59
60



180x182mm (150 x 150 DPI)

Manuscript

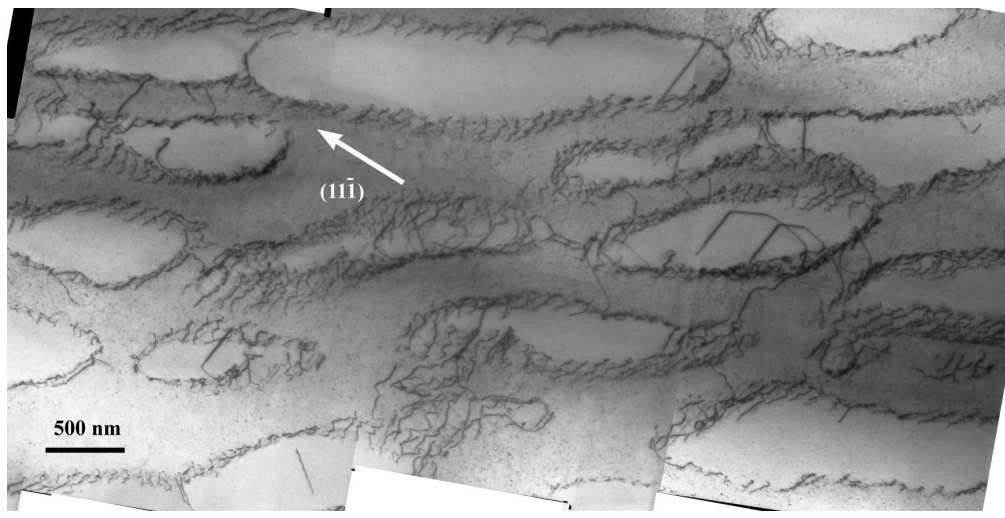
1
2
3
4
5
6
7
8
9
10
11
12
13
14
15
16
17
18
19
20
21
22
23
24
25
26
27
28
29
30
31
32
33
34
35
36
37
38
39
40
41
42
43
44
45
46
47
48
49
50
51
52
53
54
55
56
57
58
59
60



254x190mm (96 x 96 DPI)

View Only

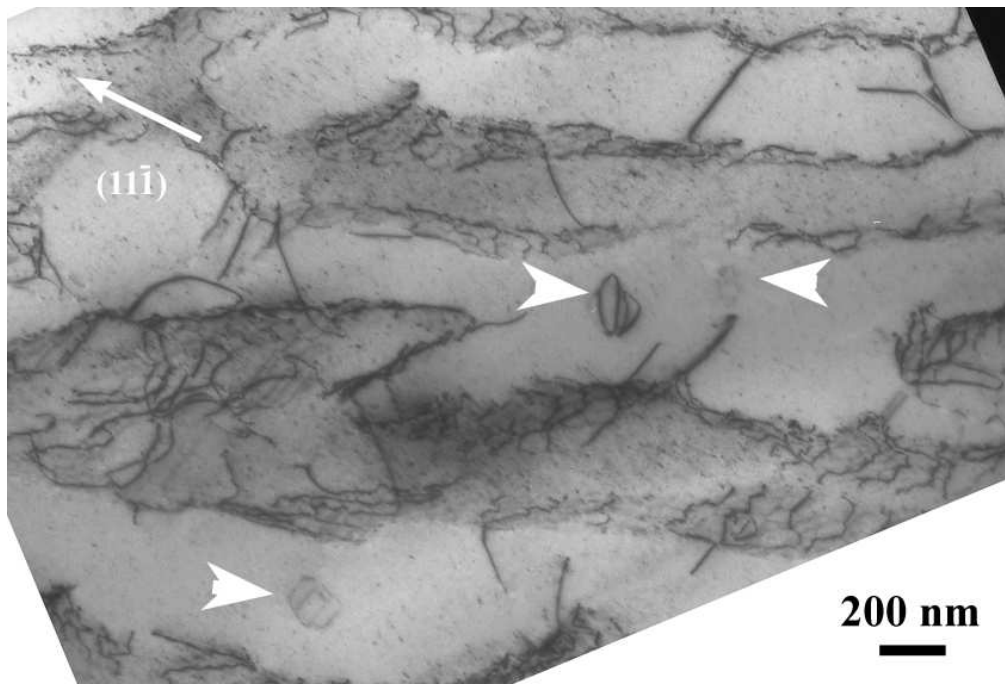
1
2
3
4
5
6
7
8
9
10
11
12
13
14
15
16
17
18
19
20
21
22
23
24
25
26
27
28
29
30
31
32
33
34
35
36
37
38
39
40
41
42
43
44
45
46
47
48
49
50
51
52
53
54
55
56
57
58
59
60



293x147mm (150 x 150 DPI)

Review Only

1
2
3
4
5
6
7
8
9
10
11
12
13
14
15
16
17
18
19
20
21
22
23
24
25
26
27
28
29
30
31
32
33
34
35
36
37
38
39
40
41
42
43
44
45
46
47
48
49
50
51
52
53
54
55
56
57
58
59
60



141x96mm (150 x 150 DPI)

Review Only